ResearchGate

See discussions, stats, and author profiles for this publication at: https://www.researchgate.net/publication/30053632

High-Resolution Ion-Imaging Studies of the Photodissociation of the BrCl + Cation †

ARTICLE *in* THE JOURNAL OF PHYSICAL CHEMISTRY A · SEPTEMBER 2004

Impact Factor: 2.69 · DOI: 10.1021/jp049238q

CITATIONS
13

READS
33

7 AUTHORS, INCLUDING:

Andre T J B Eppink
Radboud University Nijmegen
30 PUBLICATIONS **1,953** CITATIONS
SEE PROFILE

Angela Marcela Coroiu
University of Leuven
12 PUBLICATIONS **77** CITATIONS
SEE PROFILE

David H Parker
Radboud University Nijmegen
204 PUBLICATIONS **4,818** CITATIONS
SEE PROFILE

Available from: Andre T J B Eppink
Retrieved on: 27 January 2016

PCCP

High resolution ion imaging studies of the photodissociation of the Br_2^+ cation

Marco Beckert, Stuart J. Greaves† and Michael N. R. Ashfold*

School of Chemistry, University of Bristol, Bristol, UK BS8 1TS.
E-mail: mike.ashfold@bris.ac.uk; Fax: +44 (0)117 9250612; Tel: +44 (0)117 9288312/3

Received 23rd September 2002, Accepted 21st November 2002
First published as an Advance Article on the web 29th November 2002

We demonstrate the potential of velocity map ion imaging methods for high resolution studies of the photofragmentation of a state selected molecular ion, Br_2^+. $^{79}Br_2^+$ cations were prepared in the $v^+ = 1$ levels of both spin–orbit components of the X $^2\Pi_g$ ground state by $2+1$ resonance enhanced multiphoton ionisation (REMPI) of jet-cooled, isotopomer-selected $^{79}Br_2$ molecules at an excitation wavelength of 263.012 nm. The subsequent photolysis of these state selected ions was then investigated in the wavelength range $372 < \lambda_{phot} < 432$ nm by imaging the resulting $^{79}Br^+$ ions. Use of a home-built Pockels cell assembly allowed measurement of images with and without λ_{phot} present, on successive laser shots. The resulting difference image allows clear visualisation of the parent ion fragmentation, free from unintended fragment ion signal induced by the REMPI preparation step. The images reveal participation of dissociation channels yielding Br^+ ions in both their ground ($^3P_2$) and first excited ($^3P_1$) spin–orbit states, together with ground state Br atoms. No fragmentation channels involving formation of spin–orbit excited Br($^2P_{1/2}$) atoms are found to be active in this range of photolysis wavelengths. Image analysis yields a precise value for the bond strength of the Br_2^+ cation, in both spin–orbit components of its ground electronic state: $D_0[^{79}Br_2^+(X\ ^2\Pi_{1/2,g})] = 23528.1 \pm 0.6$ cm^{-1} and $D_0[^{79}Br_2^+(X\ ^2\Pi_{3/2,g})] = 26345 \pm 2$ cm^{-1}, and thus a refined measure of the spin–orbit splitting in the ground state Br_2^+ cation: $A = 2817 \pm 3$ cm^{-1}.

Introduction

The development of ion imaging methods,[1] especially the velocity mapping variant of the technique,[2] has enabled a wealth of new and detailed investigations of contemporary problems in chemical physics, spanning detailed studies of gas phase molecular photodissociation[3–6] and photoionisation[7] processes, and inelastic and reactive collisions.[8,9] The product of principal interest in most such studies reported to date has been a neutral species, which has been ionised at source—with quantum state specificity—*via* an appropriate resonance enhanced multiphoton ionisation (REMPI) scheme, and then detected with a time and position sensitive detector. Analysis of the resulting image can afford a particularly direct visualisation of the velocity (*i.e.* speed and angular) distribution of the probed product and, through energy and momentum conservation arguments, of the undetected partner species.[10] More elaborate experiments, involving judicious combinations of photolysis and/or REMPI probe laser propagation directions and polarisations can reveal higher moments of the recoil distribution, notably measures of the product orientation and alignment.[4,11]

The present study introduces a variant of previous imaging studies of molecular photofragmentation processes. The precursor of interest is a state-selected molecular ion—Br_2^+ in these demonstration experiments—in a well defined electronic, spin–orbit and vibrational state. Fragmentation is induced by one photon absorption, yielding an ionic product (Br^+) that can be imaged directly. In as much that the fragment of interest is created charged, and thus directly amenable to imaging without further interaction with radiation, the present work has parallels with recent studies of ion pair product formation in the photolysis of, for example, methyl chloride.[12] Imaging products arising from such ion fragmentation processes has been reported previously, but such observations have generally been the accidental (and poorly controlled) by-product of traditional neutral molecule photofragmentation studies involving intense photolysis and/or probe laser pulses.[13] Here, as in earlier studies of state-selected ion molecule reactions,[14] we use REMPI to prepare parent ions of interest with electronic, fine structure and vibrational quantum state specificity. Such methods will be applicable for most, if not all, molecules whose REMPI excitation spectra show well-resolved Rydberg structure, and rely on the strong propensity for core-conserving $\Delta v = 0$ transitions in the final one photon excitation from the resonance enhancing Rydberg state into the ionisation continuum of the parent molecule.[15]

The ground state of the Br_2^+ cation is an inverted $^2\Pi_g$ state derived from the electronic configuration $...\sigma_g^2\pi_u^4\pi_g^3\sigma_u^0$ (henceforth written simply in terms of the respective orbital occupancies, *i.e.* 2430). Ionisation energies for both spin–orbit components of this state have been derived, with progressively improved precision, from traditional photoelectron spectroscopy (PES),[16–19] threshold PES[20] and, most recently, two colour $2+1'$ pulsed field ionisation (PFI)[21] studies; the respective adiabatic ionisation potentials (IP = $84\,828 \pm 2$ cm^{-1} [$^2\Pi_{g,3/2}$] and $87\,648 \pm 2$ cm^{-1} [$^2\Pi_{g,1/2}$]) and the ground state spin–orbit splitting (2820 ± 4 cm^{-1}) are thus now established.[21] *Ab initio* calculations confirm that the dominant electronic configuration contributing to the first excited state, the A $^2\Pi_u$ state, in the vertical Franck–Condon region is 2340, but also reveal an avoided crossing between the $^2\Pi_{u,1/2}$ component of this state and the (2421) $^4\Sigma^-_u$ state at larger internuclear separation.[22] This interaction has been invoked as the cause of the surprisingly different spectroscopic parameters for the $^2\Pi_{u,3/2}$ and $^2\Pi_{u,1/2}$ components of the A state deduced from analysis

† Permanent address: Department of Chemistry, University of Durham, South Road, Durham, UK DH1 3LE.

 DOI: 10.1039/b209310n

This journal is © The Owner Societies 2003

of portions of the Br_2^+(A–X) dispersed emission spectrum.[23–25] Combining the findings of the most recent of these analyses[25] with the ground state ionisation thresholds determined by PFI[21] yields adiabatic ionisation energies for the A $^2\Pi_{u,3/2}$ and A $^2\Pi_{u,1/2}$ thresholds of 101 206 cm^{-1} and 101 715 cm^{-1}, respectively, and an excited state spin–orbit splitting of just 510 cm^{-1}. We note that this value is substantially smaller than those suggested by the earlier analyses of Br_2^+(A–X) dispersed emission[23,24] and of the threshold photoelectron spectrum of Br_2.[20] Here we present the first high resolution photochemical studies of Br_2^+, focussing on aspects of its fragmentation behaviour following excitation at energies just above its lowest dissociation threshold. The present work concentrates on demonstrating the direct, precise determination of the bond dissociation energies of both spin–orbit components of the X $^2\Pi_g$ ground state of the Br_2^+ cation. Future analyses will provide detailed information about product spin–orbit branching ratios and the recoil anisotropy of these various fragmentation channels, as a function of excitation energy. The study offers a new route to high resolution studies of the photodissociation dynamics of state selected molecular ions.

Experimental

The high-resolution ion imaging spectrometer used in the present work has been described in detail previously.[3] Briefly, a pulsed, skimmed, supersonic beam of Br_2 molecules (50 Torr seeded in 1 atm of Ar carrier gas) directed along the Z axis was crossed at right angles by the output of two pulsed tuneable lasers that counter-propagate along the X axis. Laser 1, an Nd:YAG pumped frequency doubled dye laser (Spectra-Physics GCR-250 plus Sirah Cobra Stretch, yielding an output bandwidth <0.1 cm^{-1} in the visible), was used to prepare Br_2^+ ions by a one colour $2+1$ REMPI process. Wavelengths (in air) and the corresponding vacuum wavenumbers of all photons used in this study were measured using a wavemeter (Coherent, WaveMaster). All results presented here employed a preparation wavelength $\lambda_{prep} \sim 263.012$ nm in air ($2\bar{\nu} \sim 76\,019.4$ cm^{-1} in vacuum), with the $v' = 1$ level of the Rydberg state labelled [1/2]4d;0_g[26] of the $^{79}Br_2$ isotopomer providing resonance enhancement at the two photon energy. This shorthand descriptor implies that the Rydberg state comprises a d electron orbiting the $^2\Pi_{g,1/2}$ ion core, that the quantum number for the total electronic angular momentum along the bond axis, $\Omega = 0$, and that the overall state symmetry is gerade. The resulting ions were photolysed with the output of laser 2, a second tuneable laser system (Spectra-Physics GCR-170 plus PDL-2 dye laser), which provided linearly polarised radiation in the wavelength range $372 < \lambda_{phot} < 432$ nm, with ε_{phot} perpendicular to the molecular beam axis and parallel to the plane of the detector ($\varepsilon_{phot}//Y$). Typical pulse energies used in the present work were 10–20 μJ and 50–100 μJ for lasers 1 and 2, respectively. Both pulses were focussed (20 cm f.l. lenses) into the interaction region, with the laser pulse used to induce ion fragmentation delayed ~5 ns relative to the Br_2^+ ion preparation pulse. The resulting ions were extracted, along Z, under velocity map imaging conditions using an electric field custom designed so as to optimise the resolution of the spectrometer. 860 mm downstream from the interaction volume the ion cloud impinges on the front face of a position sensitive detection system comprising of a pair of microchannel plates and a phosphor screen, which is read out by a CCD camera equipped with a fast intensifier (Photonic Science) that is gated to the time-of-flight (TOF) of $^{79}Br^+$ ions.

The experimental arrangement incorporates one additional, important feature. In nearly all cases, parent ion preparation by REMPI will be accompanied by some unwanted fragment ion formation. To discriminate against this unwanted background $^{79}Br^+$ signal from laser 1 alone, a Pockels cell (Cleveland Crystals, model QX 1020 comprising a KD*P crystal, no index matching fluid and enclosed by uncoated spectrosil B windows) and a linear polarizer were inserted in the beam path immediately before the lens with which λ_{phot} is focused into the interaction region. The linear polariser was aligned so as to transmit λ_{phot} in its 'natural' polarisation state, *i.e.* with $\varepsilon_{phot}//Y$. Application of the appropriate half-wave retardation voltage, $V_{\lambda/2}$, for the KD*P crystal at the photolysis wavelength of interest causes ε_{phot} to be rotated through 90°; in this state the fixed polarizer blocks λ_{phot}. A suitable power supply was thus used to switch λ_{phot} on and off on successive laser shots, at the 10 Hz repetition rate of the pump and probe lasers. Each ion image resulting from a single laser shot was processed with an event counting, centroiding algorithm provided with the commercial camera software DaVis (LaVision) running on a PC, and the resulting counts accumulated in two alternate buffers according to whether λ_{phot} was present or not. Images for each status were accumulated over 10^4 laser shots, and the required Br^+ image induced by λ_{phot} obtained from the difference.

Results and discussion

Several factors need consideration when planning high resolution imaging studies of fragments resulting from photolysis of a molecular ion. Appropriate spectrometer design, the use of event counting methods for image collection, and accurate image processing strategies will all aid optimal image resolution, but various spectroscopic aspects can also be influential. Br_2 was chosen as a suitable test system for a number of reasons. Its excitation spectrum shows well resolved Rydberg vibronic structure.[26] This is important if, as here, it is intended to use one-colour $2+1$ REMPI to prepare the parent ion, and to rely on the expected propensity for core-conserving $\Delta v = 0$ transitions from the intermediate Rydberg level to ensure that these ions are formed, predominantly, in a single, well-defined electronic, spin–orbit and vibrational state.[27] Numerous previous REMPI–time-of-flight mass spectrometry (TOFMS) and REMPI–photoelectron spectroscopy (PES) studies have shown that multiphoton excitation with just λ_{prep} can often lead to fragment ion formation.[28] Such fragmentation can arise in many different ways. For example, it can occur in cases where λ_{prep} happens to be resonant with an electronic transition of the parent ion, and the resulting excited state of the ion is dissociative (or predissociative). Fragment ions are often also seen in cases where the resonance enhancing state of the neutral molecule is of mixed Rydberg, valence and/or ion-pair character. Further photon absorption can lead to 'super-excited' states lying at energies above the first ionisation limit. These can ionise, directly or indirectly (autoionise). They can also dissociate—either to ionic and neutral fragments, or to yield neutral fragments one (or more) of which are electronically excited. Further absorption of one or more λ_{prep} photons by such neutral photofragments constitutes yet another one-colour route to forming fragment ions.[29] Any such mechanisms that cause fragment ion formation by λ_{prep} alone will hamper observation of the sought after fragment ion signal induced by λ_{phot}, and degrade the signal to noise of the required two-colour fragment ion images.

Br_2 has many of the necessary attributes for this demonstration study. It is a diatomic molecule, which dissociates to two atomic fragments. The Br and Br^+ products have ^2P and ^3P ground states, respectively, each of which exhibit substantial, resolvable, spin–orbit splitting (Br: $E(^2P_{3/2}) = 0$ cm^{-1}, $E(^2P_{1/2}) = 3685.24$ cm^{-1}; Br^+: $E(^3P_2) = 0$ cm^{-1}, $E(^3P_1) = 3136.4$ cm^{-1}, $E(^3P_0) = 3837.5$ cm^{-1} [30]). Momentum matching the products is thus unambiguous. Previous $2+1$ REMPI studies of Br_2 have identified a number of resonances which result in, primarily, parent ion formation,[26] and that demonstrate the

expected propensity for $\Delta v = 0$ core conserving transitions in the final ionisation step.[27] The first of these studies guided our choice of a resonance associated with the [1/2]4d;$0_g \leftarrow$ X;0_g two-photon transition. Br_2 exists in three isotopomers, however, and the respective origin bands of the [1/2]4d;$0_g \leftarrow$ X;0_g transition of each of these overlap one another to the extent that it is not possible to excite just a single isotopomer. Such would be desirable when striving for the highest resolution images since, though use of a time-gated image intensifier allows one to monitor just $^{79}Br^+$ or $^{81}Br^+$ fragment ions, the partner neutral fragment could be of either mass. The resulting momentum (and thus recoil velocity) partitioning is slightly different in the two cases, leading to some image blurring. Fortunately, the vibrational term values of the different parent isotopomers are sufficiently different that the corresponding 2 + 1 REMPI spectra *via* the respective $v' = 1$ levels of the [1/2]4d;0_g state are fully resolved when using a jet-cooled molecular beam of Br_2 molecules. This is illustrated in Fig. 1, which also displays the TOF mass spectra of the ions formed when exciting *via* the respective maxima of the REMPI transitions associated with each isotopomer. Fig. 1 also includes a simulated band contour of the [1/2]4d;$0_g \leftarrow$ X;0_g ($v' = 1 \leftarrow v'' = 0$) two photon transition of $^{79}Br_2$. This simulation employs rotational constants for the ground state neutral[31] and the $v^+ = 1$ level of the ion[25] (which is assumed to be a reasonable mimic for those of the $v' = 1$ level of the [1/2]4d;0_g Rydberg state) and, on the basis of the observed band envelopes, assumes that the transition is carried solely by the zero rank component of the two photon transition tensor. The remaining adjustable parameters are the parent rotational temperature (which our various trial simulations suggest is ~8 K) and the linewidth associated with each individual rovibronic transition. The displayed best-fit simulation (by eye) was obtained using a Lorentzian lineshape of 0.25 cm^{-1} (convoluted with an assumed Gaussian lineshape of 0.15 cm^{-1} (FWHM) representing the effective two photon laser linewidth). If we assume that predissociation of the resonance enhancing [1/2]4d;0_g $v = 1$ Rydberg level is the major contributor to the homogeneous broadening, we obtain an estimate of ~20 ps for this excited state lifetime.

Images presented in this work were all recorded while exciting at the peak of the $^{79}Br_2$ resonance at $\lambda_{prep} = 263.012$ nm ($\bar{\nu}_{prep} = 38\,009.7$ cm^{-1}) and monitoring the $^{79}Br^+$ fragment ion. As Fig. 1 illustrates, the partner fragment produced at this particular wavelength must be a ^{79}Br atom. Fig. 2 compares raw images of the $^{79}Br^+$ fragment ions formed as a result of the limited amount of unwanted fragmentation that accompanies one colour 2 + 1 REMPI of Br_2 with $\bar{\nu}_{prep} = 38\,007.5$ cm^{-1} (Fig. 2(b)) with that observed upon introduction of an additional photolysis laser photon at $\bar{\nu}_{phot} = 26\,600$ cm^{-1} (Fig. 2(a)). These two images were obtained by accumulating counts from alternate laser shots (with the photolysis beam successively blocked and transmitted through use of the Pockels cell as described above) in separate buffers. The two images are thus automatically self-normalised, and the difference image (Fig. 2(c)) obtained by subtracting Fig. 2(b) from Fig. 2(a) gives a high resolution measure of the recoil (speed and angular distribution) of the various $^{79}Br^+ + {}^{79}Br$ fragmentation channels that are active when Br_2^+ ions formed by 2 + 1 REMPI at $\bar{\nu}_{prep} = 38\,007.5$ cm^{-1} are photolysed at $\bar{\nu}_{phot} = 26\,600$ cm^{-1}. Note the improved clarity of the innermost ring that is overlapped by the isotropic one colour signal in Fig. 2(a). Further analysis requires reconstruction of the 3-D velocity distribution from the accumulated 2-D ion images as described previously[32] using an algorithm based on the filtered back projection method of Sato *et al.*[33]

The left hand column in Fig. 3 shows the difference image recorded at $\bar{\nu}_{phot} = 26\,600$ cm^{-1} (Fig. 3(c)), together with those measured at two other photolysis wavenumbers ($\bar{\nu}_{phot} = 25\,400$ and $26\,000$ cm^{-1}). To the right, we show the

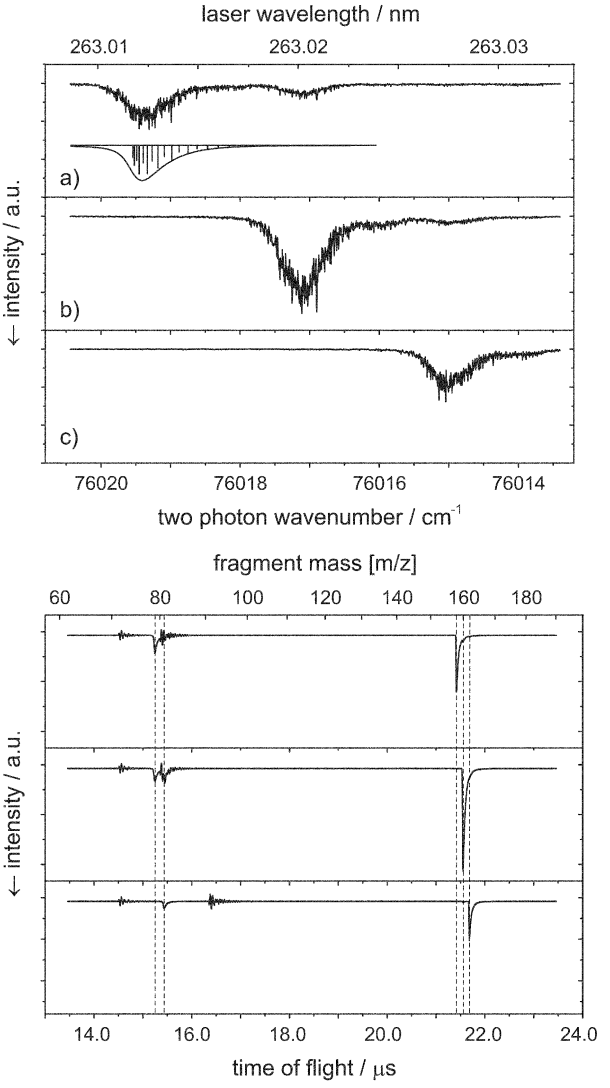

Fig. 1 2 + 1 REMPI spectra of the [1/2]4d;$0_g \leftarrow$ X;0_g ($v' = 1 \leftarrow v'' = 0$) two photon transition of Br_2 obtained by monitoring ions with (a) m/z 158 ($^{79}Br_2^+$), (b) m/z 160 ($^{79}Br^{81}Br^+$) and (c) m/z 162 ($^{81}Br_2^+$). The companion time-of-flight spectra of the resulting ions are shown alongside. The inset to (a) shows a spectral simulation (stick spectrum and band contour) obtained assuming that the two photon transition is carried solely by the zero rank component of the two photon transition tensor, ground and excited state rotational constants $B'' = 0.0820$ cm^{-1} (ref. 31) and $B' = 0.0872$ cm^{-1} (ref. 25), respectively, and a rotational temperature $T_{rot} = 8$ K. The individual rovibronic linewidths are modelled by convoluting a 0.15 cm^{-1} (FWHM) Gaussian function to represent the effective two-photon laser bandwidth and a 0.25 cm^{-1} (FWHM) Lorentzian.

associated speed distributions obtained by integrating over all angles after reconstruction of the corresponding 3-D velocity distribution. All images recorded at low photolysis wavenumber (*e.g.* the image for $\bar{\nu}_{phot} = 25\,400$ cm^{-1}) show a single ring, which the following analysis will show to arise from near threshold dissociation of $^{79}Br_2^+$ molecules in their $^2\Pi_{1/2,g}$ state and with vibrational quantum number $v^+ = 1$, yielding ground state fragments, *i.e.*

$$^{79}Br_2^+(^2\Pi_{1/2,g})_{v^+=1} + h\nu \rightarrow {}^{79}Br^+(^3P_2) + {}^{79}Br(^2P_{3/2}) \quad (1)$$

This ring expands with increasing photon energy and first one, and then a second, additional peaks appear in the image. These additional peaks are associated with, respectively, the equivalent fragmentation originating from the ground spin–orbit state of the parent ion:

$$^{79}Br_2^+(^2\Pi_{3/2,g})_{v^+=1} + h\nu \rightarrow {}^{79}Br^+(^3P_2) + {}^{79}Br(^2P_{3/2}) \quad (2)$$

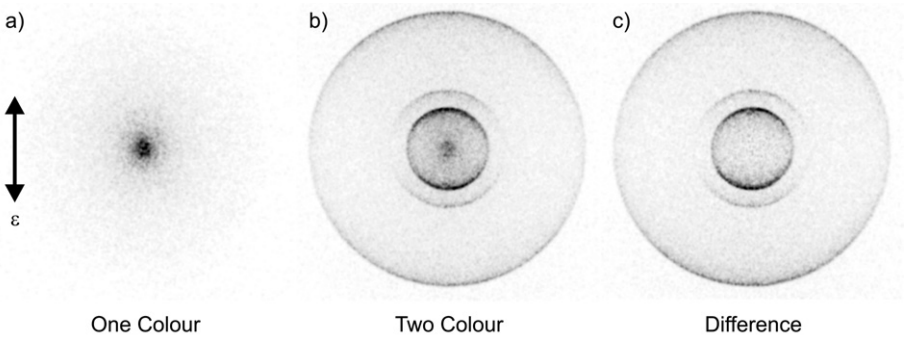

Fig. 2 Raw ion images of obtained $^{79}Br^+$ ions obtained following (a) $2+1$ REMPI at 263.012 nm and (b) upon addition of a second laser pulse with $\bar{\nu}_{phot} = 26\,600$ cm^{-1}, delayed by $\delta t \sim 5$ ns with respect to the REMPI laser. Both laser beams were linearly polarised, with their respective polarisation vectors ε aligned perpendicular to the molecular beam axis and parallel to the plane of the detector, *i.e.* aligned along Y and as indicated by the double headed arrow in (a). (c) depicts the difference image obtained by subtracting the one colour image (Fig. 2(a)) from the two colour image (Fig. 2(b)). For display purposes, each image has been plotted using the full dynamic range of the grey scale.

and the analogue of process (1) but yielding $^{79}Br^+$ ions in their first spin–orbit excited state:

$$^{79}Br_2{}^+(^2\Pi_{1/2,g})_{v^+=1} + h\nu \rightarrow {}^{79}Br^+(^3P_1) + {}^{79}Br(^2P_{3/2}). \quad (3)$$

In the remainder of this paper we concentrate on detailed analysis of these speed distributions, and the way they can be used to derive a precise value for the bond dissociation energy of the $Br_2{}^+$ cation. The present experiments provide three different routes to the bond strength of the $Br_2{}^+$ cation.

The first method relies on the fact that the molecule displays electronic absorption at wavelengths corresponding to the lowest dissociation threshold, so a reasonably precise value for this threshold energy can be obtained simply by recording images as a function of decreasing $\bar{\nu}_{phot}$ (in 5 cm^{-1} intervals), finding the photon energy at which the ring associated with product channel (1) last appears as a small central spot ($\bar{\nu}_{threshold} \sim 23\,165$ cm^{-1}), and then adding a best estimate of the internal energy of the initial state selected $Br_2{}^+$ molecules.

Method 2 we have demonstrated previously, when determining an accurate value for D_0(I–Br).[32] As before, we fit these measured velocity distributions in terms of a function

$$S(r) = \sqrt{\frac{8\ln 2}{\pi}}\left\{\sum_{i=1}^{2}\left(\frac{S_i}{w_{1/2}}\exp\left[-4\ln 2((r-r_i)/w_{1/2})^2\right] + \frac{\bar{S}_i}{w_{1/2}}\exp\left[-4\ln 2((r-\bar{r}_i)/w_{1/2})^2\right]\right)\right\}, \quad (4)$$

where i labels the two spin–orbit states of the $Br_2{}^+$ ion ($i = 1$ ($^2\Pi_{1/2}$), $i = 2$ ($^2\Pi_{3/2}$)), r is the radius in pixels, S_i and $\bar{S}_i$ are the intensities of peaks involving formation of, respectively,

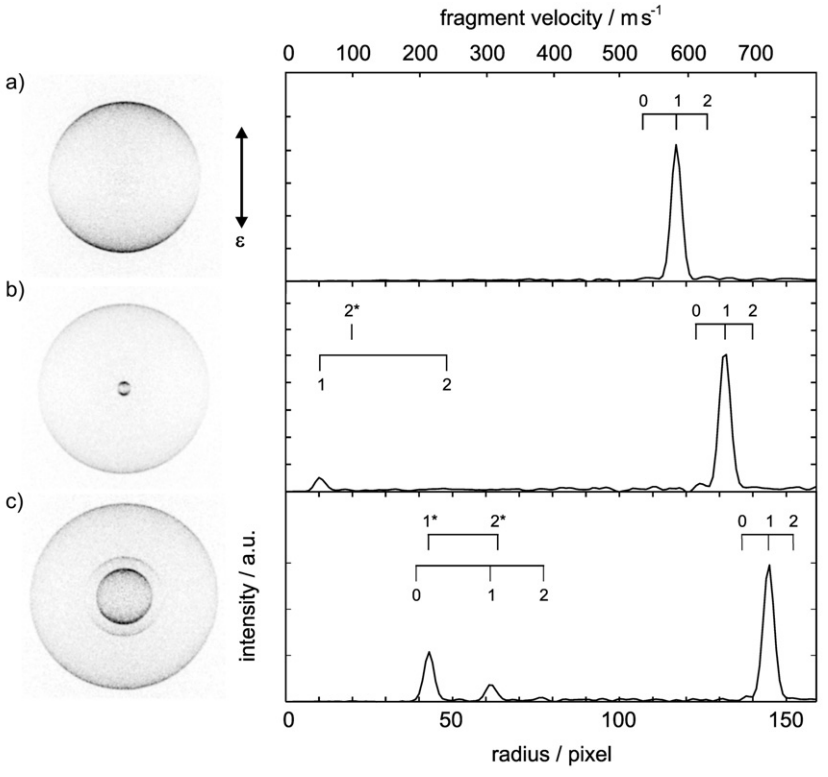

Fig. 3 Difference images for the $^{79}Br^+$ fragment ions resulting from dissociation of $^{79}Br_2{}^+$ parent ions following excitation at (a) 25 400, (b) 26 000 and (c) 26 600 cm^{-1}. ε denotes the electric vector of the photolysis radiation. The speed distributions derived from analysis of the corresponding reconstructed 3-D velocity distributions are shown alongside. The combs arranged above the speed distributions indicate the velocities of products arising from the indicated v^+ levels *via* channels (1)—the fastest peak in each distribution—and, where appropriate, eqns. (2) and (3) following photolysis of $Br_2{}^+$ parent ions in specified spin–orbit and vibrational states. Peaks arising from fragmentation channel (3) are indicated by asterisks.

ground ($^3P_2$) and spin–orbit excited ($^3P_1$) Br^+ ions, and $w_{1/2}$ is the width (FWHM) of the Gaussian function used to describe the velocity distribution associated with each particular parent → product channel. r_i and $\bar{r}_i$ depend on the Br^+ fragment velocities according to

$$r_i(\alpha, D_i) = \frac{1}{\alpha m_{Br}}[h\nu - D_i]^{1/2} \quad (5a)$$

and

$$\bar{r}_i(\alpha, D_i) = \frac{1}{\alpha m_{Br}}[h\nu - (D_i + E_{so}(Br^+))]^{1/2}, \quad (5b)$$

where α is the proportionality constant linking the fragment recoil velocity and the image radius, $m_{Br} = 78.918$ u, and D_i is the dissociation energy of a Br_2^+ ion with internal energy $E_{int,i}$. As before, the fits were performed using the non-linear Levenberg–Marquardt method.[34] The correlation between α and D_i in eqn. (5) can be avoided, and α determined independently, in those images that show products from both channels (eqn. (1)) and (eqn. (3)). Since $E_{so}(Br^+)$ is known precisely, we can use energy and momentum conservation in such cases to determine

$$\alpha = \sqrt{\frac{E_{so}}{m_{Br}(r_1^2 - r_2^2)}}. \quad (6)$$

This forms the basis for the third method for determining $D_e(Br_2^+)$ we discuss later. Focussing on Method 2, the fitting returns r values for the maxima of the various peaks in each velocity distribution, with sub-pixel resolution. The dissociation energies, D_i, can then be determined from the y-axis intercepts of linear fits to plots of photon energy *versus* the square of the corresponding r_i values as illustrated in Fig. 4. This method relies on proper experimental design, in as much that the image radius must scale linearly with the fragment recoil velocity, but does not necessarily require determination of α. The extrapolation to zero fragment kinetic energy also means that, unlike Method 1, it is not essential that the molecule absorbs and dissociates at threshold. Method 2 is thus applicable to molecules with dissociation limits that lie outside the Franck–Condon window, or that have an energy barrier in the dissociation coordinate. Clearly, however, the accuracy of the determination will be highest when, as here, it is possible to include data from rings with small r.

Our previous study of this type involved a jet-cooled sample of IBr. Individual rings in the images of the resulting Br fragments were modelled in terms of a Boltzmann distribution of thermally populated parent rotational states, each with its own rovibrational energy, and each of which was convoluted by an instrumental lineshape when fitting the experimentally measured peak shape in the fragment speed distribution. In contrast, the present study involves state selected Br_2^+ ions. The REMPI excitation scheme *via* the $v' = 1$ level of the [1/2] 4d;0_g Rydberg state encouraged us to expect formation of parent ions in the excited X $^2\Pi_{1/2,g}$ spin–orbit state and with $v^+ = 1$. Image analysis supports this expectation. The combs arranged above the deduced speed distributions in Fig. 3 confirm the Franck–Condon diagonal nature of the final one photon ionisation process, but also reveal that there is some probability for forming Br_2^+ ions in the lower (X $^2\Pi_{3/2,g}$) spin–orbit state, again with $v^+ = 1$. Such behaviour is most readily explained by assuming some core-mixing in the resonance enhancing Rydberg level, as suggested previously by Koenders *et al.* to account for the unexpected complexity of certain of their measured 2 + 1 REMPI-photoelectron spectra of Br_2.[27] All of the peaks in the present Br^+ speed distributions are found to fit well to single Gaussian functions, with $w_{1/2} \sim 4.0$ pixels (FWHM). This value matches closely the FWHM used to fit the contribution from just a single parent quantum state in our earlier studies of IBr photolysis, employing the same experimental conditions, implying that the ions prepared in the present study are not just electronic, spin–orbit and vibrational state selected, but also involve a high degree of rotational state selection. To explain this, we note that the [1/2]4d;$0_g \leftarrow$ X;0_g ($v' = 1 \leftarrow v'' = 0$) two photon transition (Fig. 1(a)) of jet-cooled $^{79}Br_2$ molecules comprises a simple series of Q branch lines. The relatively narrow homogeneous width of each of these lines ensures that excitation at the peak of the band envelope will select a sub-set of rotational levels (centred at $J'' \sim 5$). The observation that all peaks in the speed distributions are well described by single narrow Gaussian functions is then understandable if the final one photon ionisation step from the [1/2]4d;0_g $v' = 1$ level shows a high propensity for transitions that conserve the rotational angular momentum of the core—thereby resulting in formation of ions in a narrow distribution of rotational states with quantum number $N^+ \sim 5$. This observation hints that, in favourable cases, high resolution ion imaging methods might be able to complement REMPI-PES methods[28] in shedding light on rotational state propensities in molecular photoionisation processes.

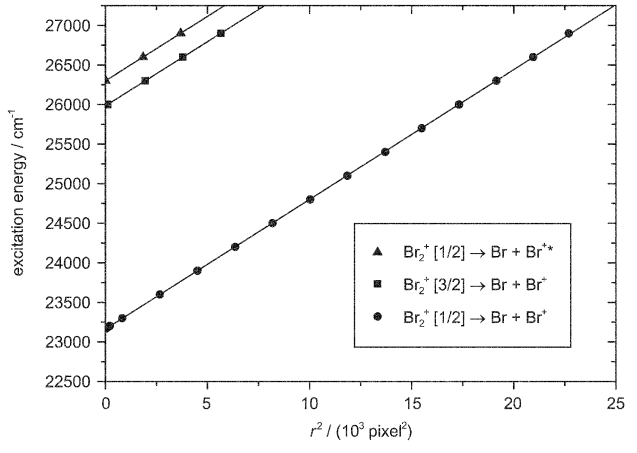

Fig. 4 Plot of excitation energy *versus* squared best-fit image radius r^2 (in pixels squared, proportional to the kinetic energy) for Br^+ products arising from photodissociation of state selected Br_2^+ ions *via* processes (1, ●), (2, ■) and (3, ▲). The threshold energies for the different fragmentation channels are deduced *via* linear fitting of the respective data sets.

Returning to Fig. 4, the analysis of the most extensive sequence of images (associated with fragmentation channel (1)) yields a y-axis intercept: $D_{i=1} = 23\,160.4 \pm 2.2$ cm^{-1}—in excellent accord with the limit deduced by Method 1. Extrapolation of the smaller data sets yields threshold energies of 25 982.9 cm^{-1} and 26 298.5 cm^{-1} for channels (2) and (3), respectively. Each is mutually consistent, within the uncertainty limits, with documented values of the spin–orbit splittings in Br_2^+(X)[21] and Br^+.[30] To convert these data to dissociation energies measured from the corresponding $v^+ = 0$, $N^+ \sim 0$ levels (or to the corresponding D_e values) we have to correct for the internal energy of the initial state selected $^{79}Br_2^+$ molecules and, if necessary, for any spin–orbit excitation of the products. Focussing on channel (1), for example,

$$D_e(^{79}Br\text{–}^{79}Br^+(^2\Pi_{1/2,g})) = D_{i=1} + E_{int}[^{79}Br_2^+(X^2\Pi_{1/2,g} v^+ = 1, N^+ \sim 5)] \quad (7a)$$

and

$$D_0(^{79}Br\text{–}^{79}Br^+(^2\Pi_{1/2,g})) = D_e(^{79}Br\text{–}^{79}Br^+(^2\Pi_{1/2,g})) - E_{int}[^{79}Br_2^+(X^2\Pi_{1/2,g} v^+ = 0, N^+ \sim 0)]. \quad (7b)$$

The E_{int} values in eqn. (7) can be calculated from the very precise spectroscopic constants of $^{79}Br^{81}Br^+$ reported by Zackrisson.[25] Somewhat surprisingly, this analysis (which we have confirmed by refitting the published line listings) shows that the low v^+ levels of the two components of the X $^2\Pi_g$ state have identical rovibrational term values—at least for the low v^+ levels investigated,[25] and that are relevant for the present work. After scaling for the appropriate reduced mass, we obtain $E_{int}(v^+ = 1,\ N^+ \sim 5) = 551.3$ cm^{-1} and $E_{int}(v^+ = 0,\ N^+ = 0) = 183.5$ cm^{-1} for the $^{79}Br_2$ isotopomer, and thus $D_0[^{79}Br_2{}^+(^2\Pi_{1/2,g})] = 23\,528.2 \pm 2.2$ cm^{-1}. The more limited amount of data for photolysis involving ground spin–orbit state ions means that $D_0[^{79}Br_2{}^+(^2\Pi_{3/2,g})] \sim 26\,351$ cm^{-1} cannot be defined to quite the same precision. Clearly, however, Method 2 could be used to obtain a yet more precise value of $D_0(Br_2{}^+(X^2\Pi_{3/2,g}))$ were we to record a similarly extensive set of high resolution images following dissociation of comparably well state-selected $Br_2{}^+$ ions in the ground spin–orbit state.

As discussed previously,[32] the foregoing analysis has the advantage that it involves a global fit of many data sets, thereby serving to smooth out errors associated with any individual data point. Implicit in the analysis, however, is the assumed invariance of α for the given set of operating conditions (flight path, extraction voltages *etc*.) The third approach, in contrast, determines the various D_i values by fitting to an individual measurement. Consider an image such as that shown in Fig. 3(c). The deduced speed distribution contains peaks attributable to dissociation channels (1) and (3), which originate from the same sub-set of rovibrational state selected $^2\Pi_{1/2,g}$ parent ions, and which dissociate to limits whose energy separation is known precisely. Fitting in terms of Gaussian functions yields S_i, $w_{1/2}$ and, most importantly, the peak centre r_i values for each of these peaks. Inserting these latter values into eqn. (6) yields a best-fit value of α (and its associated uncertainty) and thence, *via* eqn. (5), a value for D_i. This can then be converted to $D_0[Br_2{}^+(^2\Pi_{1/2,g})]$ or $D_e[Br_2{}^+(^2\Pi_{1/2,g})]$ given the appropriate E_{int} values, as before.

We find no systematic difference in the FWHM values of the Gaussian used to fit peak (2)—which we associate with photolysis of $Br_2{}^+(X\ ^2\Pi_{3/2,g})$ parent ions—and those for peaks (1) and (3). This encourages our assumption of a similar propensity for $\Delta N \sim 0$ transitions in the photoionisation process leading to formation of these ground state ions. For any one image, therefore, the r values for the centres of peaks corresponding to channels (1) and (2), together with α and the two D_i values, allow determination of the energy separation between the $^2\Pi_{3/2}$ and $^2\Pi_{1/2}$ components of ground state $Br_2{}^+$ ions with $v^+ = 1$ and $N^+ \sim 5$. Table 1 lists the results of such analyses of images recorded at $\bar{\nu} = 26\,600$ and $26\,900$ cm^{-1}. Given the above assumption, E_{int} will be the same for each channel and this energy separation can thus be associated solely with the spin–orbit splitting, $A(Br_2{}^+(X))$. This final method of analysis yields final error weighted values of $D_{i=1} = 23\,160.3 \pm 0.6$ cm^{-1}, $D_{i=2} = 25\,977 \pm 2$ cm^{-1} and $A(Br_2{}^+) = 2817 \pm 3$ cm^{-1}. This value for the spin–orbit splitting parameter for the $Br_2{}^+(X)$ cation is in complete accord with that determined in the recent $2+1'$ PFI study of Br_2 (2820 ± 4 cm^{-1}, ref. 21).

Our best-estimate dissociation energies are: $D_0[^{79}Br_2{}^+(X\ ^2\Pi_{1/2,g})] = 23\,528.1 \pm 0.6$ cm^{-1} (in very good agreement with the values derived *via* Methods 1 and 2), $D_0[^{79}Br_2{}^+(X\ ^2\Pi_{3/2,g})] = 26\,345 \pm 2$ cm^{-1} and $D_e[Br_2{}^+(X\ ^2\Pi_{3/2,g})] = 26\,528 \pm 2$ cm^{-1}. We are not aware of any prior direct determination of the bond strength of the ground state $Br_2{}^+$ cation, but it is possible to derive a value for this quantity from the following thermodynamic cycle:

$$\begin{aligned} D_0[Br_2{}^+(X^2\Pi_{i,g})] &= D_0(Br_2(X)) + IP[Br(^2P_{3/2} \rightarrow {}^3P_2)] \\ &\quad - IP[Br_2(X, 0^+, v = 0, J = 0) \\ &\quad \rightarrow Br_2{}^+(X^2\Pi_{i,g} v^+ = 0, N^+ = 0)], \end{aligned} \qquad (8)$$

where $D_0(^{79}Br_2(X)) = 15\,894.52 \pm 0.01$ cm^{-1} (refs. 30 and 35), $IP[Br(^2P_{3/2} \rightarrow {}^3P_2)] = 95\,284.8$ cm^{-1} (ref. 30) and the threshold energies for forming $Br_2{}^+(X)$ ions in their X $^2\Pi_{3/2,g}$ and X $^2\Pi_{1/2,g}$ states have been measured as, respectively, $84\,828 \pm 2$ cm^{-1} and $87\,648 \pm 2$ cm^{-1} (ref. 21). This thermodynamic cycle yields values $D_0[Br_2{}^+(X\ ^2\Pi_{3/2,g})] = 26\,351 \pm 2$ cm^{-1} and $D_0[Br_2{}^+(X\ ^2\Pi_{1/2,g})] = 23\,531 \pm 2$ cm^{-1}, in very good accord with the present determinations. The slight differences, if significant, might be associated with the fact that the $2+1'$ PFI measurements necessarily involved use of a natural abundance sample of Br_2 molecules, an assumed correction for the field induced shift in ionisation threshold, and that the measured ionisation thresholds are for an (unspecified) distribution over populated parent rotational states rather than for $J'' = 0$ molecules.

Conclusions

We report a high resolution imaging study of fragment ions resulting from photodissociation of state selected molecular ions prepared by REMPI. The present study focuses on photolysis of $Br_2{}^+$ molecules in selected spin–orbit, vibrational and even rotational states, over the wavelength range $372 < \lambda_{phot} < 432$ nm. The analyses reported here yield precise values for the bond dissociation energies of ground state $Br_2{}^+$ molecules: $D_0[^{79}Br_2{}^+(X\ ^2\Pi_{1/2,g})] = 23\,528.1 \pm 0.6$ cm^{-1} and $D_0[^{79}Br_2{}^+(X\ ^2\Pi_{3/2,g})] = 26\,345 \pm 2$ cm^{-1}, and thus a refined measure of the spin–orbit splitting in the ground state $Br_2{}^+$ cation: $A = 2817 \pm 3$ cm^{-1}. The latter value is in excellent accord with that measured in a recent two colour $2+1'$ PFI study, and the respective dissociation energies agree well with values that can be derived from available energetic data.[21,30,35] Imaging fragments from the photolysis of state-selected cations, as demonstrated here, has a number of parallels with recent studies of the fragmentation of neutral molecules into ion pair products.[9] In both cases, quantum state resolved information about the (unobserved) partner fragment is obtained directly from analysis of the image of the nascent ionic fragment. Given the wealth of existing REMPI–photoelectron spectroscopic data demonstrating clean preparation of vibrational state selected small and medium sized molecular ions we suggest that the present experiment points the way to many new high resolution photochemical studies of molecular ions. Clearly, for heteronuclear diatomics and for polyatomic species, the method offers a route to measuring the various different fragment ion yield curves, as a function of excitation energy, and of initial vibronic state of the parent ion.

Table 1 Summary of the results of best-fit simulations of the speed distributions extracted from reconstructed images of $^{79}Br^+$ fragment ions resulting from photolysis of state-selected $Br_2{}^+$ ions. The quoted uncertainties in α and the D_i values are 1σ

$\bar{\nu}$/cm^{-1}	α/m s^{-1} pixel^{-1}	$D_{i=1}$/cm^{-1}	$D_{i=2}$/cm^{-1}	$A(Br_2{}^+(X))$/cm^{-1}
26 600	4.9890 ± 0.0004	$23\,160.4 \pm 0.6$	$25\,977 \pm 2$	2817 ± 3
26 900	4.9955 ± 0.0007	$23\,159.3 \pm 1.9$	$25\,976 \pm 6$	2817 ± 8

Acknowledgements

Funding from the EPSRC (equipment grants, a Senior Research Fellowship (MNRA) and studentships (MB and SJG)) and the Commission of the European Communities [TMR contract no. ERB-4061-PL-97-0264 (IMAGINE)] is gratefully acknowledged. Preliminary REMPI–PES studies of Br_2 were carried out in the laboratory of Prof. T. N. Kitsopoulos at ULF-FORTH under the IHP-ARI programme of the EC (contract no. HPRI-CT-1999-00074). We are also very grateful to Bristol colleagues K. N. Rosser and Drs A. J. Orr-Ewing and C. M. Western, and past-colleagues Drs E. R. Wouters (now at Stanford Research Institute) and E. Wrede (now at University of Durham), for their many and varied contributions to the work described herein.

References

1 D. W. Chandler and P. L. Houston, *J. Chem. Phys.*, 1987, **87**, 1445.
2 A. T. J. B. Eppink and D. H. Parker, *Rev. Sci. Instrum.*, 1997, **68**, 3477.
3 E. Wrede, S. Laubach, S. Schulenburg, A. Brown, E. R. Wouters, A. J. Orr-Ewing and M. N. R. Ashfold, *J. Chem. Phys.*, 2001, **114**, 2629 and references therein.
4 E. R. Wouters, M. Beckert, L. J. Russell, K. N. Rosser, A. J. Orr-Ewing, M. N. R. Ashfold and O. S. Vasyutinskii, *J. Chem. Phys.*, 2002, **117**, 2087 and references therein.
5 A. V. Demyanenko, A. B. Potter, V. Dribinski and H. Reisler, *J. Chem. Phys.*, 2002, **117**, 2568.
6 T. P. Rakitzis and T. N. Kitsopoulos, *J. Chem. Phys.*, 2002, **116**, 9228 and references therein.
7 E. Surber and A. Sanov, *J. Chem. Phys.*, 2002, **116**, 5921 and references therein.
8 K. T. Lorenz, D. W. Chandler and G. C. McBane, *J. Phys. Chem. A*, 2002, **106**, 1144 and references therein.
9 X. H. Liu, R. L. Gross and A. G. Suits, *J. Chem. Phys.*, 2002, **116**, 5341 and references therein.
10 *Imaging in Chemical Dynamics*, ACS Symp. Ser. 770, ed. A. G. Suits and R. E. Continetti, American Chemical Society, Washington, D.C., 2001.
11 E. R. Wouters, M. Ahmed, D. S. Peterka, A. S. Bracker, A. G. Suits and O. S. Vasyutinskii, in ref. 10, pp. 238–84.
12 X. H. Liu, R. L. Gross and A. G. Suits, *Science*, 2001, **294**, 2527 and references therein.
13 D. H. Parker, B. L. G. Bakker, P. C. Samartzis and T. N. Kitsopoulos, *J. Chem. Phys.*, 2001, **115**, 1205 and references therein.
14 See, for example W. E. Conaway, T. Ebata and R. N. Zare, *J. Chem. Phys.*, 1987, **87**, 3447; W. E. Conaway, T. Ebata and R. N. Zare, *J. Chem. Phys.*, 1987, **87**, 3453.
15 M. N. R. Ashfold and J. D. Howe, *Annu. Rev. Phys. Chem.*, 1994, **45**, 57 and references therein.
16 D. C. Frost, C. A. McDowell and D. A. Vroom, *J. Chem. Phys.*, 1967, **46**, 4255.
17 A. W. Potts and W. C. Price, *J. Chem. Soc., Faraday Trans.*, 1971, **67**, 1242.
18 A. B. Cornford, D. C. Frost, C. A. McDowell, J. L. Ragle and I. A. Stenhouse, *J. Chem. Phys.*, 1971, **54**, 2651.
19 H. van Lonkhuyzen and C. A. de Lange, *Chem. Phys.*, 1984, **89**, 313.
20 A. J. Yencha, A. Hopkirk, A. Hiraya, R. J. Donovan, J. G. Goode, R. R. J. Maier, G. C. King and A. Kvaran, *J. Phys. Chem.*, 1995, **99**, 7231.
21 T. Ridley, D. A. Beattie, M. C. R. Cockett, K. P. Lawley and R. J. Donovan, *Phys. Chem. Chem. Phys.*, 2002, **4**, 1398.
22 K. Balasubramanian, *Chem. Phys.*, 1988, **119**, 41.
23 T. Harris, J. H. D. Eland and R. P. Tuckett, *J. Mol. Spectrosc.*, 1983, **98**, 269.
24 P. A. Hamilton, *Chem. Phys. Lett.*, 1987, **140**, 591.
25 M. Zackrisson, *J. Mol. Spectrosc.*, 1994, **163**, 371.
26 R. J. Donovan, A. C. Flexen, K. P. Lawley and T. Ridley, *Chem. Phys.*, 1998, **226**, 217.
27 B. G. Koenders, G. J. Kuik, K. E. Drabe and C. A. de Lange, *Chem. Phys. Lett.*, 1988, **147**, 310.
28 C. A. de Lange, *Adv. Chem. Phys.*, 2001, **117**, 1 and references therein.
29 P. C. Samartzis, T. N. Kitsopoulos and M. N. R. Ashfold, *Phys. Chem. Chem. Phys.*, 2000, **2**, 453.
30 NIST Atomic Spectra Database, http://physics.nist.gov/cgi-bin/AtData/main_asd.
31 K. P. Huber and G. Herzberg, *Molecular Spectra and Molecular Structure, IV. Constants of Diatomic Molecules*, van Nostrand, New York, 1979.
32 E. Wrede, S. Laubach, S. Schulenburg, A. J. Orr-Ewing and M. N. R. Ashfold, *Chem. Phys. Lett.*, 2000, **326**, 22.
33 Y. Sato, Y. Matsumi, M. Kawasaki, K. Tsukiyama and R. Bersohn, *J. Phys. Chem.*, 1995, **99**, 16 307.
34 W. H. Press, S. A. Teukolsky, W. T. Vetterling, B. P. Flannary, *Numerical Recipes in C*, Cambridge University Press, Cambridge, 1994.
35 R. F. Barrow, T. C. Clark, J. A. Coxon and K. K. Yee, *J. Mol. Spectrosc.*, 1974, **51**, 428.